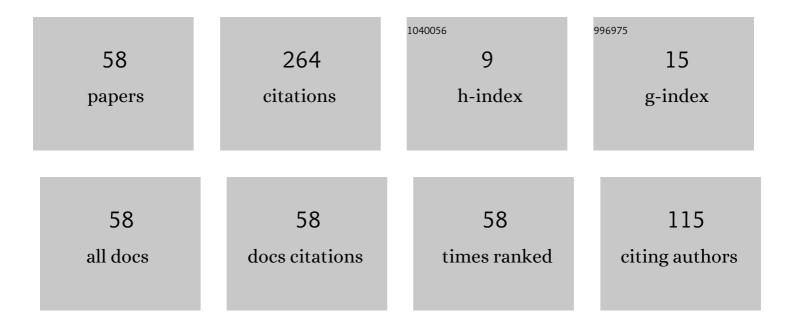
## List of Publications by Year in descending order

Source: https://exaly.com/author-pdf/2400675/publications.pdf Version: 2024-02-01



KIINTI

#	Article	IF	CITATIONS
1	Monte Carlo Simulation of Clothed Skin Exposure to Electromagnetic Field With Oblique Incidence Angles at 60 GHz. Frontiers in Public Health, 2022, 10, 795414.	2.7	7
2	Two-Way Power Divider With Wide Tunable Power Ratio Range for Weighted-Polarization MIMO Antenna in BAN Radios at 2.45 GHz. IEEE Antennas and Wireless Propagation Letters, 2022, 21, 1333-1337.	4.0	4
3	Multivariate Regression Analysis of Skin Temperature Rises for Millimeter-Wave Dosimetry. IEEE Transactions on Electromagnetic Compatibility, 2022, 64, 941-950.	2.2	4
4	Editorial: Human Exposure to New-Emerging Electric, Magnetic and Electromagnetic Fields. Frontiers in Public Health, 2022, 10, 894624.	2.7	6
5	Human Skin Exposure to Terahertz Waves from 0.1 to 1 THz: Statistical Assessments Using Multilayered Planar Models. , 2022, , .		3
6	Effect of Incidence Angle on the Spatial-Average of Incident Power Density Definition to Correlate Skin Temperature Rise for Millimeter Wave Exposures. IEEE Transactions on Electromagnetic Compatibility, 2021, 63, 1709-1716.	2.2	14
7	A Novel Estimation Method of Local Peak SAR for 5G Sub-6GHz Antennas using MIMO-OTA. , 2021, , .		2
8	Quantitative Comparison of Power Densities Related to Electromagnetic Near-Field Exposures With Safety Guidelines From 6 to 100 GHz. IEEE Access, 2021, 9, 115801-115812.	4.2	15
9	Measurement of Rice factor for In-Body Radios at 950 MHz in Indoor Environment. , 2021, , .		0
10	Relationship between Local Peak SAR and MIMO Performance for 5G Sub-6GHz Antennas. , 2021, , .		0
11	Intercomparison of Calculated Incident Power Density and Temperature Rise for Exposure From Different Antennas at 10–90 GHz. IEEE Access, 2021, 9, 151654-151666.	4.2	20
12	Computational Comparison of Power Density Definitions in the Proximity of Antennas for the Assessment of Human Exposure to EMF above 6 GHz. , 2020, , .		2
13	Experimental Validations on Low-Error Estimation Models in Determining the Maximum Specific Absorption Rate of Multi-Antenna Mobile Handsets. , 2019, , .		0
14	Averaging Area for Transmitted Power Density Correlated to Temperature Elevation on Human Skin Surface due to RF Exposure at 60 GHz. , 2019, , .		0
15	A New Measurement Technique to Determine the Maximum SAR of Multiple-Antenna Transmitters Using \$K\$-Order Models and Scalar E-Field Probes. , 2019, , .		0
16	\$K\$ -Order Estimation Technique for Determining the Maximum Electric Fields of Multiple-Antenna Transmitters in Compliance Tests. IEEE Transactions on Antennas and Propagation, 2019, 67, 5602-5613.	5.1	4
17	Relationship between power density and surface temperature elevation for human skin exposure to electromagnetic waves with oblique incidence angle from 6 GHz to 1 THz. Physics in Medicine and Biology, 2019, 64, 065016.	3.0	49
18	Design of Human-Skin Equivalent Phantom for Evaluating the Surface Temperature Elevation due to Millimeter Wave Exposure. , 2019, , .		1

#	Article	IF	CITATIONS
19	Determining the Maximum Local Specific Absorption Rate of a Multiple-Antenna Transmitter Using K-Order Electric Field Models. , 2019, , .		0
20	A Novel Estimation Technique using K-Order Models to Evaluate the Maximum Electric Field of Multiple-Antenna Transmitters. , 2019, , .		0
21	Estimation of Transmitted Power Density from Temperature Experiment for EMF Exposure Assessment at 60 GHz. , 2019, , .		0
22	Accuracy of Incident Power Density Measured Using Reconstructing Algorithm for Compliance Assessment of Devices in Near-Field at Millimeterwave Frequencies. , 2019, , .		1
23	Error Analysis of a Near-Field Reconstruction Technique Based on Plane Wave Spectrum Expansion for Power Density Assessment Above 6 GHz. IEEE Access, 2019, 7, 11591-11598.	4.2	22
24	EMF Exposure from 5G Equipment at Millimeter Wave Frequencies. , 2018, , .		2
25	A Waffle-Iron Ridge Guide with Combined Fast- and Slow-Wave Modes for Array Antenna Applications. IEICE Transactions on Communications, 2018, E101.B, 349-356.	0.7	1
26	Dual-Discrete Processing for Bit-Error-Rate OTA Testing in Shadowing-Fading BAN Channels. IEEE Antennas and Wireless Propagation Letters, 2017, 16, 1200-1204.	4.0	5
27	A phase shifter using waffle-iron ridge guides and its application to a beam steering antenna. IEICE Communications Express, 2017, 6, 188-193.	0.4	0
28	Decoupling stub-loaded parallel dipole array with orthogonal polarization. IEICE Communications Express, 2017, 6, 97-102.	0.4	0
29	Regression-Based Channel Capacity for the Evaluation of 2×2 MIMO Antennas. IEICE Transactions on Communications, 2017, E100.B, 323-335.	0.7	5
30	Wavelength Analysis Using Equivalent Circuits in a Fast and Slow Wave Waffle-Iron Ridge Guide. IEICE Transactions on Communications, 2017, E100.B, 219-226.	0.7	1
31	Bit-error-rate OTA testing of BAN antennas based on shadowing-fading hybrid effects. , 2016, , .		1
32	Weighted-polarization wearable antenna for on-body dynamic channels. IEICE Communications Express, 2016, 5, 189-194.	0.4	2
33	High efficiency mw-band dielectric resonator rectenna using distributed capacitors. IEICE Communications Express, 2016, 5, 254-259.	0.4	2
34	Optimum phase shift applied to weighted-polarization MIMO antenna in various use scenarios. IEICE Communications Express, 2016, 5, 266-271.	0.4	1
35	A method of controlling the base station correlation for MIMO-OTA based on Jakes model. IEICE Communications Express, 2016, 5, 297-302.	0.4	2
36	Three-dimensional MIMO-OTA calibration to achieve the Gaussian angular power spectra in elevation. IEICE Communications Express, 2016, 5, 394-400.	0.4	12

#	Article	IF	CITATIONS
37	Three-Dimensional Over-The-Air Assessment for Vertically Arranged MIMO Array Antennas. IEICE Transactions on Communications, 2016, E99.B, 167-176.	0.7	6
38	Weighted-Polarization Wearable MIMO Antenna with Three Orthogonally Arranged Dipoles Based on RF Signal Processing. IEICE Transactions on Communications, 2016, E99.B, 58-68.	0.7	11
39	Analysis of the Body Proximity Cross-Polarization Power Ratio in a human walking motion. , 2015, , .		0
40	The 3-axis polarization antenna using Disk-Loaded Monopole stacked with Patch antenna in PCB. , 2015, ,		2
41	A simultaneous conjugate-matching algorithm for <i>N</i> -element array antennas. IEICE Communications Express, 2015, 4, 327-332.	0.4	0
42	Analysis of the body proximity cross-polarization power ratio in a human walking motion. , 2015, , .		2
43	A polarization-controlled MIMO antenna with an optimum phase shift in accordance with various use scenarios. , 2015, , .		2
44	Dual-polarized turn-style patch antenna for wearable applications. , 2015, , .		1
45	Three-axis decoupling stub-loaded parallel dipole array with tri-orthogonal polarization directivity. , 2015, , .		1
46	Disk-loaded monopole stacked with patch antenna. , 2015, , .		4
47	A base station correlation-controlled bilateral emulator for MIMO-OTA. , 2015, , .		1
48	Experiments of a polarization-controlled active antenna to enhance BAN on-body link in human dynamic channels. , 2015, , .		3
49	Rice Channel Realization for BAN Over-The-Air Testing Using a Fading Emulator with an Arm-Swinging Dynamic Phantom. IEICE Transactions on Communications, 2015, E98.B, 543-553.	0.7	12
50	An 8×8 MIMO 3-axis weighted polarization active antenna for wearable radio applications. , 2014, , .		9
51	A sequential automatic impedance-matching algorithm to achieve simultaneous complex-conjugate condition in multi-element antennas. , 2014, , .		2
52	Three-dimensional OTA design considerations based on MIMO antenna radiation and multipath interactions. , 2014, , .		0
53	On-body polarization-controlled active antenna to enhance signal power in human dynamic channels. , 2014, , .		4
54	Over-the-air assessment for 2-dimensional arrangement MIMO array antennas. , 2014, , .		3

 $Over-the-air\ assessment\ for\ 2-dimensional\ arrangement\ MIMO\ array\ antennas.\ ,\ 2014,\ ,\ .$ 54

#	Article	IF	CITATIONS
55	BAN Over-the-Air testing using an arm-swinging dynamic phantom. , 2013, , .		0
56	Shadowing-fading BER characterization of BAN antennas based on realistic walking models. , 2013, , .		2
57	BAN-OTA testing using a fading emulator with an arm-swinging dynamic phantom. , 2013, , .		1
58	Shadowing-Fading BER Characterization of a BAN Diversity Antenna Based on Statistical Measurements of the Human Walking Motion. IEICE Transactions on Communications, 2013, E96.B, 2530-2541.	0.7	10